minerals

MDPI

Article

Sr-Nd-Pb-Ca Isotopes of Holocene Basalts from Jingpohu, NE China: Implications for the Origin of Their Enriched Mantle Signatures

Feixiang Wei [1,2,*], Bo Pan [1,2] and Jiandong Xu [1,2]

[1] Jilin Changbaishan Volcano National Observation and Research Station, Institute of Geology, China Earthquake Administration (CEA), Beijing 100029, China; dujushi1981@163.com (B.P.); xujiandong@ies.ac.cn (J.X.)
[2] Key Laboratory of Seismic and Volcanic Hazards, China Earthquake Administration (CEA), Beijing 100029, China
* Correspondence: weifeixiang@ies.ac.cn

Abstract: The geochemistry on Holocene lavas from the Jingpohu volcanic field in NE China are compared with other Cenozoic lavas from across the back-arc rift of NE China, in order to constrain their enriched mantle sources. Holocene lavas within Jingpohu volcanic field comprise two separate "Crater Forest" (CF) and "Frog Pool" (FP) volcanic areas. FP lavas have lower MgO, CaO, and heavy rare earth elements and higher Al_2O_3, Na_2O, K_2O, and large-ion lithophile elements than CF lavas. Yet, both CF and FP lavas share similar isotopic signatures, with depleted Sr and Nd isotopes ($^{87}Sr/^{86}Sr$ = 0.703915–0.704556, $^{143}Nd/^{144}Nd$ = 0.512656–0.512849) and unradiogenic Pb isotopes ($^{208}Pb/^{204}Pb$ = 37.79–38.06, $^{207}Pb/^{204}Pb$ = 15.45–15.54, $^{206}Pb/^{204}Pb$ = 17.49–18.15), similar to oceanic island basalts. An important new constraint for the Jingpohu lavas lies in their Ca isotopes of $\delta^{44/40}Ca$ from 0.63‰ to 0.77‰, which are lower than that of the bulk silicate earth (0.94 ± 0.05‰). By comparing the isotopic signatures of sodic lavas with that of the potassic lavas across NE China, we propose a three-component mixing model as the source for the sodic lavas. In consistence with geophysical results, we propose that subducting Pacific plate induces asthenospheric mantle upwelling of an upper depleted mantle (DM), including subducted ancient sediments (EM I), which partially melted upon ascent. These primary melts further interacted with the lithospheric mantle (EM II), before differentiating within crustal magma chambers and erupting.

Keywords: Jingpohu volcano; EM I; EM II; Ca isotope; Pacific plate

check for updates

Citation: Wei, F.; Pan, B.; Xu, J. Sr-Nd-Pb-Ca Isotopes of Holocene Basalts from Jingpohu, NE China: Implications for the Origin of Their Enriched Mantle Signatures. *Minerals* **2021**, *11*, 790. https://doi.org/10.3390/min11080790

Academic Editor: Martin Bromann Klausen

Received: 31 May 2021
Accepted: 18 July 2021
Published: 21 July 2021

Publisher's Note: MDPI stays neutral with regard to jurisdictional claims in published maps and institutional affiliations.

Copyright: © 2021 by the authors. Licensee MDPI, Basel, Switzerland. This article is an open access article distributed under the terms and conditions of the Creative Commons Attribution (CC BY) license (https://creativecommons.org/licenses/by/4.0/).

1. Introduction

Enriched mantle components typically have low $^{143}Nd/^{144}Nd$, variable $^{87}Sr/^{86}Sr$, and high $^{208}Pb/^{204}Pb$ and $^{207}Pb/^{204}Pb$ ratios (at a given value of $^{206}Pb/^{204}Pb$) [1] and can be further subdivided into an EM I with relatively low $^{87}Sr/^{86}Sr$ ratios and an EM II with relatively high $^{87}Sr/^{86}Sr$ ratios [1]. Within the Cenozoic back-arc rift of NE China (Figure 1), both potassic and sodic lava suites have enriched chemical as well as isotopic signatures that are arguably derived from enriched mantle sources [2–4]. In recent decades, an increasing number of studies indicate that the potassic suites can be explained by a mixture of an enriched EM I and a depleted mantle (DM) component [4,5]. However, the chemical and isotopic signatures of sodic suites appear to require an additional enriched EM II source [6].

Several geodynamic models have tried to locate the origins of the enriched mantle components beneath NE China, including the metasomatized lithosphere [9–11], recycled sediments brought up by a mantle plume [3], and enriched fluids in the mantle transition zone released by the dehydration of the present Pacific slab and/or earlier subducted plates [4,6,12,13]. While it is widely accepted that the westward subduction of the Pacific plate plays a signifi-

cant dynamic role in triggering recent Cenozoic volcanism in NE China [11–15], the origins of their enriched components are still under intense debate [2,3,10].

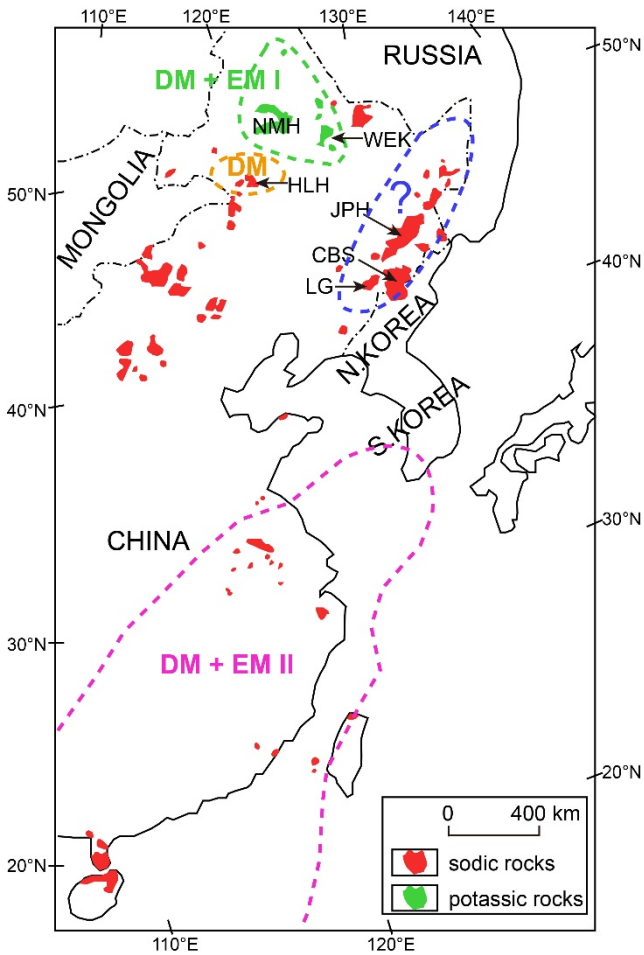

Figure 1. Spatial distribution of Cenozoic basalts across east China (modified from [4,7]), color-coded as either potassic or sodic. While all appear to share a depleted upper mantle (DM) source, the potassic Nuomihe (NMH) and Wudalianchi–Erkeshan–Keluo (WEK) volcanic fields (inside green dashed line) incorporate an enriched EM I component, while volcanoes across a broad SE China region (inside magenta dashed line) are characterized by an EM II component. Halaha (HLH) lava (inside yellow dashed line) has neither of these additional enriched mantle signatures [8]. The sources of the sodic lavas in the blue dashed line are still under debate. Other sodic volcanic fields: JPH = Jingpohu, CBS = Changbaishan, LG = Longgang.

Spatially, the sodic lavas from Jingpohu, Changbaishan, and Longgang volcanic fields lie between the potassic DM + EM I domain and the DM + EM II domain across east China (Figure 1). Therefore, these may provide new insights into these enriched mantle components. Recently, Bai et al. [13] reviewed the geochemical data of the lavas from Jingpohu volcanic field and suggested that previous interpretations of these lead to wrong conclusions regarding their magma sources. Furthermore, only one sample from the "Frog Pool" volcanic area had credible isotopic data and was, thereby, insufficient to constrain its magma sources. In this paper, we rectify this through an additional 11 Holocene basalt samples from the Jingpohu volcanic field with special attention on its "Frog Pool" volcanic area. The study, furthermore, includes high-precision chemical and isotopic data, which will help constrain the sources of enriched mantle components beneath NE China.

2. Geological Background

Despite being located up to 2400 km behind the west Pacific subduction zone, many intraplate volcanoes, during the Cenozoic, have formed across NE China, e.g., Jingpohu, Changbaishan, and Wudalianchi volcanoes, inside what is best described as a back-arc rift setting. Spatially, the province's potassic rocks are mainly restricted within the northernmost part of China, such as Wudalianchi–Erkeshan–Keluo (WEK) and Nuomihe volcanic fields (Figure 1), while sodic lavas, including the Changbaishan, Longgang, and Jingpohu volcanic fields, scatter across a much larger area to the south and east of these (Figure 1). As revealed through tomographic imaging, the subducted slab of the Pacific plate levels out along the base of the upper mantle [14,15] and could, thereby, likely play an additional role in supplying magma source components to the intraplate volcanism. However, whether the Pacific slab can still contribute to Cenozoic volcanism in NE China remains controversial [2,10,15].

The Jingpohu volcanic field is located close to Dunhua–Mizhi fault and erupted from Eocene to Holocene, with the most recent eruptions 5500–5200 year before present (BP) [16,17]. Magnetotelluric (MT) low-resistivity [18,19] and seismic low-velocity [20,21] anomalies at depths of 8–16 km and 30–100 km record likely partial melting beneath the Jingpohu volcanoes but at a lower degree than below the Changbaishan volcano [21]. During a 4-month mobile seismic survey in 2002, 39 seismic events mostly within the Jingpohu [22] indicated that the Jingpohu volcanoes may still erupt.

Thirteen young Holocene volcanic craters are found within the XiaoBeihu Forest and range in size from being dozens of meters to more than 400 m in diameter and from less than 10 m to more than 100 m in depth. While 11 of these craters cluster within a southern "Crater Forest" (CF) volcanic area, only two craters comprise a separate "Frog Pool" (FP) volcanic area in the north (Figure 2). A larger lava flow from the CF craters snaked down a river valley, blocked an older channel of the Mudan River and, thereby, formed the Jingpohu Lake. Located approximately 15 km apart, a correspondingly smaller lava flow emanates from the crater pair within the FP volcanic area. Even if carbon-14 ages show that the two volcanic areas erupted synchronously at 5200–5500 year BP [16,17], the petrology and geochemistry of the lavas from the two volcanic areas differ [23].

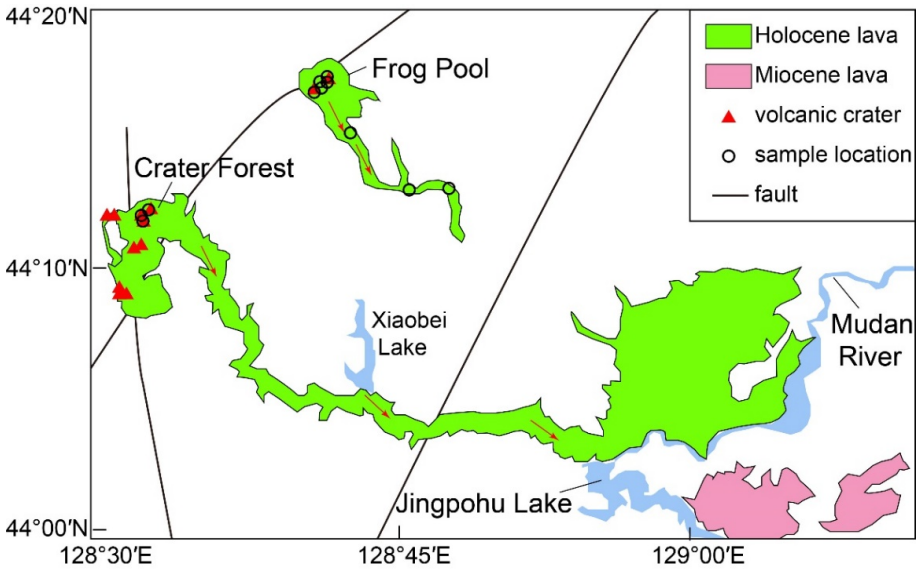

Figure 2. Distribution of Holocene lavas and craters within the Jingpohu volcanic field.

3. Analytical Method

Eleven lava samples were selected for geochemical analysis, including 8 from the FP and 3 from the CF volcanic area. The altered surfaces of collected samples were cut off, and only fresh parts crushed to an approximately 5 mm sized fragments by a steel jaw crusher. Fragments were hand-picked and ground into fine powder in an agate ball mill. Powders were then dried at 105 °C for 12 h in oven before being processed for whole-rock major and trace elements, as well as Sr-Nd-Pb-Ca isotopic analyses at the Sample Solution Lab in Wuhan, China.

3.1. Major and Trace Elements

Whole-rock major element analyses were conducted on a Primus II X-ray fluorescence machine (XRF; Rigaku, Japan). Firstly, approximately 1 g of dried sample powder was precisely weighted and fused at 1000 °C for 2 h inside a muffle furnace. After being cooled, the fused sample was weighted again for calculating any loss on ignition (LOI). Then, 0.6 g of the cooled sample was mixed with 6.0 g cosolvent ($Li_2B_4O_7$:$LiBO_2$:LiF = 9:2:1) and 0.3 g oxidant (NH_4NO_3) in a Pt crucible and melted at 1150 °C for 14 min. Finally, the remelted sample was cooled into a flat disc for XRF analysis. For quality control, two Chinese national geological reference materials GBW07105 (basalt) and GBW07111 (granodiorite) were measured and found in good agreement with suggested values. Duplicate measurements of sample WJ-11 also demonstrate good reproducibility of the analytical method.

Whole-rock trace element analyses were performed on an Agilent 7700e inductively coupled plasma mass spectrometer (ICP-MS). Approximately 50 mg samples were weighed and dissolved in Teflon bombs with 1 mL HNO_3 and 1 mL HF. These Teflon bombs were secured in stainless steel pressure jackets and heated for more than 24 h at 190 °C in an oven. After cooling, the Teflon bombs were carefully opened and evaporated to incipient dryness at 140 °C, and then, 1 mL HNO_3 was added and again evaporated to dryness in order to remove fluorides from the initial HF dissolution. Afterwards, 1 mL HNO_3, 1 mL MQ water, and 1 mL internal standard solution (1 ppm In) were added to the sample, sealed, and kept in an oven at 190 °C for more than 12 h. Finally, the solutions were transferred to a polyethylene bottle and diluted to 100 g by adding 2% HNO_3 for the ICP-MS analysis. Based on measurements of the standard AGV-2, BHVO-2, BCR-2, and RGM-2 and duplicate measurement of sample WJ-11, standard deviation is estimated to be <6% from suggested values for most elements, while the reproducibility of most elements is <7%. Total procedural blanks yielded element concentrations that are significantly lower than those of the Jingpohu samples.

3.2. Sr-Nd-Pb-Ca Isotopes

3.2.1. Chemical Separation

Digestion and column chemistry were employed to separate Sr-Nd-Pb-Ca elements for isotopic analysis. A total of three digestions were conducted, one for separating Sr and Nd, one for Pb, and another for Ca. For Sr and Nd separations, approximately 100 mg of dried sample powder was digested using the same method as for the trace element digestion described above. Sample solutions were loaded with 2.5 M HCl into ion-exchange columns packed with AG50W resin. Strontium fractions were eluted with 2.5 M HCl, and REE cuts were collected using 4 M HCl. Then, Sr fractions were purified in a second column loaded with Sr-specific resin, and REE cuts were loaded in a third column with Ln resin in order to separate the Nd. Another digestion of 100 mg sample was performed for the separation of Pb. These digested solutions were loaded with 1M HBr into columns with AG resin. After removing undesirable matrix elements with 1 M HBr, Pb fractions were eluted using 6 M HCl. Calcium separation required another digestion of approximately 50 mg sample using the same method. An aliquot sample solution containing 40 μg Ca was loaded into the PFA column with 250 μL DGA resin. The matrix was removed by 4 M HNO_3, and Ca fractions were collected with MQ water. The collected Ca fractions were evaporated to dryness and dissolved in 2% HNO_3 in order to achieve 10 ppm Ca solutions for MC-ICP-MS analysis.

3.2.2. Mass Spectrometry

The Sr-Nd-Pb isotope analyses were performed on a Neptune Plus MC-ICP-MS (Thermo Fisher), which was equipped with seven fixed electron multiplier ICs, and nine Faraday cups were fitted with 10^{11} Ω resistors. For Sr isotopic analysis, the faraday cups collected ^{83}Kr, ^{167}Er^{2+}, ^{84}Sr, ^{85}Rb, ^{86}Sr, ^{173}Yb^{2+}, ^{87}Sr, ^{88}Sr on channels L4 to H3. The Nd isotope analysis was performed by a faraday cup setting of ^{142}Nd, ^{143}Nd^{+}, ^{144}Nd, ^{145}Nd, ^{146}Nd, ^{147}Sm, ^{148}Nd, ^{149}Sm, ^{150}Nd on the channels L4 to H4. The faraday collector configuration for Pb isotopic measurements was composed of an array to monitor ^{202}Hg, ^{203}Tl, ^{204}Pb, ^{205}Tl, ^{206}Pb, ^{207}Pb, ^{208}Pb on L3 to H3. Each measurement consisted of 10 blocks of 10 cycles. Standard NIST SRM 987, JNdi-1, and NBS SRM 981 were used to evaluating the accuracy and reproducibility for Sr, Nd, and Pb isotopes, respectively.

Calcium isotope analyses were also conducted on the plasma equipped with a quartz dual cyclonic-spray chamber and a Savillex 50 uL/min PFA MicroFlow Teflon nebulizer. Usually, a 10 ppm ^{44}Ca^{+} solution can obtain a signal above 5 V. Before each injection, the sample-introduction system was cleaned with 5% HNO_3 for 2–3 min in order to keep the ^{44}Ca^{+} signal below 1 mV and, thereby, avoid cross-contamination between samples. A standard sample bracketing method was employed for correcting instrumental drift. Due to a limited solution of commonly used standard NIST SRM 915a, an in-house Alfa Ca standard solution (Lot: 9192737) was used for bracketing in this laboratory. For comparison, intermediate measurements of NIST SRM 915a were also performed, and the results were reported relative to that NIST SRM 915a by adding a conversion factor of 0.58. Consequently, Ca isotope compositions are reported as: $\delta^{44/42}Ca_{sample} = [^{44}Ca/^{42}Ca_{sample}/^{44}Ca/^{42}Ca_{NIST\ SRM\ 915a} - 1] \times 1000$. Each sample was measured 3 times. In addition, a calcium carbonate standard NIST SRM915b, a basalt rock standard BHVO-2, and seawater samples were also analyzed to evaluate both accuracy and reproducibility. The long-term average calculated $\delta^{44/42}Ca_{SRM915a}$ is 0.001 ± 0.058‰ (2 SD, n = 155).

4. Results

4.1. Petrography

All lavas are porphyritic, but with megacrysts only found within FP lavas and never in CF lavas. Many phlogopite and anorthoclase megacrysts were found inside lavas that were located along at the rim of the FP craters (Figure 3a,b), while a previous study has also found clinopyroxene megacrysts in these FP lavas [23]. Phenocrysts (<15%) in the FP lavas are otherwise mainly euhedral olivines and set in a glassy groundmass with plagioclase and olivine microlites (Figure 3c). The lavas from the CF volcanic area comprise 5–15% phenocrysts of olivine, clinopyroxene, and plagioclase set in a glassy ground mass with pyroxene, olivine, and plagioclase microlites (Figure 3d).

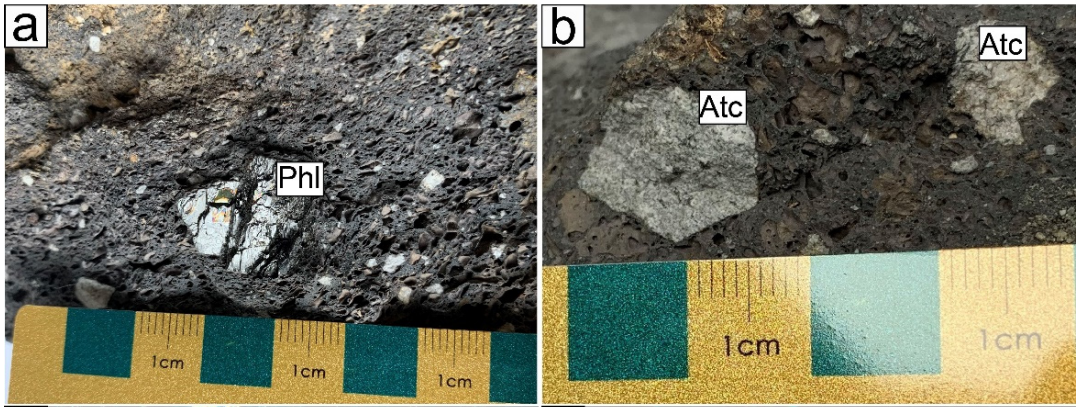

Figure 3. *Conts.*

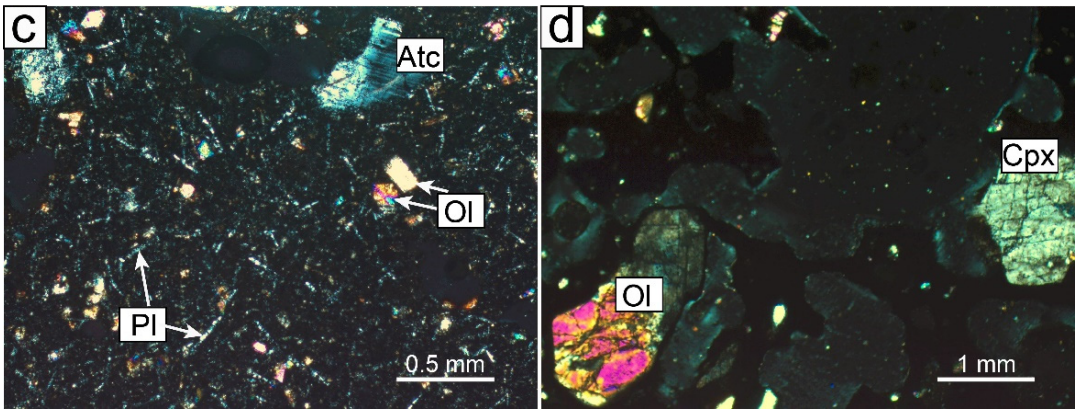

Figure 3. Photographs (**a**,**b**) and photomicrographs (**c**,**d**) of representative samples from the Jingpohu volcanic field. Phl, phlogopite; Atc, anorthoclase; Ol, olivine; Pl, plagioclase; Cpx, clinopyroxene. (**a**) Sample WJ-1 from the FP volcanic area, with a phlogopite megacryst. (**b**) Sample WJ-1 from the FP volcanic area. Anorthoclase megacrysts. (**c**) Sample WJ-3 from the FP volcanic area. Phenocrysts of olivine and anorthoclase in a ground mass consisting of volcanic glass, plagioclase, and olivine. (**d**) Sample WJ-9 from the CF volcanic area. Phenocrysts of olivine and clinopyroxene in a porphyritic texture.

4.2. Whole-Rock Major Elements

Whole-rock major elements of the Jingpohu samples are provided in Table 1 and are, for comparison, consistently plotted together with literature data of Holocene samples from Jingpohu volcanic field. The total alkali versus silica diagram (TAS), after a calculation to 100% on an anhydrous basis (Figure 4a), shows that compositions for the Holocene FP and CF volcanic areas are significantly different. These FP samples mostly cluster along the boundary between the diagram's phono-tephrite and tephri-phonolite fields, whereas CF samples mostly range across its tephrite/basanite and trachy-basalt field. All Holocene samples display K_2O/Na_2O ratios between 0.5 and 0.8 (Figure 4b), exhibiting correlations with each other and belonging to the shoshonitic series. CF samples can be further sub-divided into a low- and a high-alkali group. The three CF samples of this study all belong to the high-alkali basanitic (~15% normative olivine) group, which also has slightly lower SiO_2 contents than that of the low-alkali trachy-basaltic group. Jingpohu samples yield SiO_2 contents between 43.76% and 50.08%, and even if FP and CF samples have overlapping SiO_2 ranges, the two datasets exhibit significant differences in all other major elements except for $Fe_2O_3^{(T)}$ and TiO_2. As shown by Harker diagrams (Figure 5), FP samples have higher Al_2O_3, Na_2O, and K_2O contents and lower MgO and CaO compared to the CF samples.

Table 1. Whole-rock major and trace elements of the Holocene lavas from Jingpohu volcanic field.

Location	FP Volcanic Area								CF Volcanic Area		
Sample	**WJ-1**	**WJ-2**	**WJ-3**	**WJ-4**	**WJ-5**	**WJ-6**	**WJ-7**	**WJ-8**	**WJ-9**	**WJ-10**	**WJ-11**
(wt.%)											
SiO_2	49.47	48.88	47.68	47.35	48.20	47.52	47.94	48.38	48.12	46.97	45.21
TiO_2	1.82	1.81	1.85	1.92	1.85	1.91	1.92	1.91	1.70	1.75	1.82
Al_2O_3	16.83	16.73	16.93	17.02	16.85	17.26	17.00	17.01	15.18	15.13	14.62
Fe_2O_3(T)	10.37	10.39	10.78	10.94	10.78	11.05	10.91	10.83	10.73	11.01	11.30
MnO	0.14	0.14	0.15	0.15	0.15	0.15	0.15	0.15	0.16	0.17	0.18
MgO	4.41	4.48	4.49	4.51	4.51	4.04	4.58	4.50	8.09	8.27	9.19
CaO	5.57	5.63	5.72	5.73	5.94	5.53	5.82	5.78	7.89	8.04	8.39
Na_2O	6.08	6.06	5.94	6.03	6.28	6.62	6.18	6.15	4.89	5.02	5.21
K_2O	4.41	4.43	4.39	4.49	4.54	4.82	4.51	4.55	3.06	3.01	3.31
P_2O_5	0.98	0.99	1.06	1.03	1.03	1.10	1.02	1.01	0.85	0.88	1.01
LOI	−0.25	−0.23	0.29	0.07	−0.50	−0.54	−0.42	−0.48	−0.35	−0.35	−0.55
Total	99.83	99.31	99.27	99.22	99.61	99.46	99.62	99.79	100.32	99.90	99.67

Table 1. *Conts.*

Location	FP Volcanic Area								CF Volcanic Area		
Sample	**WJ-1**	**WJ-2**	**WJ-3**	**WJ-4**	**WJ-5**	**WJ-6**	**WJ-7**	**WJ-8**	**WJ-9**	**WJ-10**	**WJ-11**
(ppm)											
Li	12.2	12.1	10.9	10.7	11.9	11.5	11.3	11.9	12.4	11.4	11.3
Be	4.17	4.14	4.37	4.09	4.25	4.25	4.13	4.06	2.93	3.13	3.10
Sc	7.56	7.66	7.76	7.62	7.56	6.03	7.62	7.82	17.49	17.88	16.90
V	96.5	98.3	95.5	101.7	100.2	90.4	101.5	102.4	153.8	160.5	161.2
Cr	46.4	48.8	47.6	33.4	47.0	27.3	41.4	30.6	175.0	177.7	218.4
Co	32.2	32.7	33.4	34.1	32.9	32.3	33.9	33.7	44.1	45.1	48.7
Ni	50.6	52.9	52.9	46.5	46.3	37.2	49.5	44.7	151.5	156.5	200.0
Cu	23.5	23.7	23.0	22.7	23.2	21.5	23.6	23.9	33.5	36.3	34.7
Zn	126.2	125.2	132.9	131.2	128.2	134.8	131.0	126.8	105.0	104.8	109.1
Ga	27.1	27.0	28.0	27.9	27.8	28.7	27.9	27.1	22.7	22.6	22.4
Rb	90.8	90.6	88.2	87.1	85.8	86.5	86.4	87.1	63.0	59.9	58.3
Sr	1061	1068	1113	1096	1098	1172	1097	1087	1008	1023	1121
Y	21.2	21.0	21.3	21.0	21.5	20.5	21.1	20.7	26.4	25.8	26.8
Zr	378	391	401	394	393	420	388	378	264	264	282
Nb	103.1	102.9	108.8	108.2	106.3	116.0	107.0	103.4	79.3	82.1	92.5
Sn	2.46	2.53	2.57	2.51	2.32	2.52	2.56	2.50	1.91	1.88	1.94
Cs	1.20	1.17	1.20	1.14	1.16	1.22	1.14	1.17	0.94	0.91	0.93
Ba	714	713	682	704	657	677	706	706	674	668	694
La	65.6	65.3	67.4	65.7	65.4	68.5	65.2	64.1	57.4	58.3	67.7
Ce	117	117	120	117	118	123	117	115	102	103	118
Pr	13.0	12.9	13.4	13.1	13.0	13.6	13.1	12.6	11.3	11.5	13.1
Nd	49.9	49.0	51.4	50.7	50.6	53.4	50.3	49.2	42.9	44.4	50.4
Sm	9.47	9.44	9.81	9.21	9.54	10.12	9.28	9.28	8.25	8.24	9.71
Eu	2.80	2.98	2.99	3.01	3.00	3.05	2.94	2.87	2.54	2.65	2.93
Gd	7.79	7.42	7.76	7.91	7.61	7.89	7.65	7.39	7.30	7.25	8.08
Tb	0.98	0.96	1.03	1.01	0.99	1.03	1.01	0.97	1.02	1.06	1.09
Dy	4.96	4.95	5.02	4.85	4.79	5.13	4.97	5.01	5.41	5.54	6.09
Ho	0.77	0.75	0.80	0.76	0.77	0.75	0.75	0.76	0.89	0.94	0.96
Er	1.68	1.69	1.63	1.64	1.72	1.57	1.70	1.65	2.41	2.14	2.27
Tm	0.20	0.20	0.20	0.20	0.20	0.17	0.19	0.20	0.32	0.29	0.28
Yb	1.21	1.19	1.11	1.10	1.10	0.96	1.08	1.10	1.90	1.81	1.77
Lu	0.16	0.16	0.15	0.14	0.16	0.12	0.15	0.15	0.28	0.24	0.25
Hf	8.35	8.43	8.51	8.38	8.65	8.87	8.45	8.20	5.76	5.55	6.22
Ta	6.23	6.13	6.49	6.26	6.09	6.72	6.25	5.97	4.15	4.21	4.66
Tl	0.19	0.22	0.20	0.14	0.17	0.18	0.17	0.20	0.17	0.14	0.08
Pb	9.09	8.05	7.95	7.36	7.72	7.52	8.06	8.02	7.55	6.39	5.95
Th	11.66	11.34	11.05	10.87	11.02	11.47	10.83	10.49	8.81	8.09	8.83
U	2.78	2.79	2.75	2.64	2.71	2.77	2.64	2.60	2.22	1.91	2.15

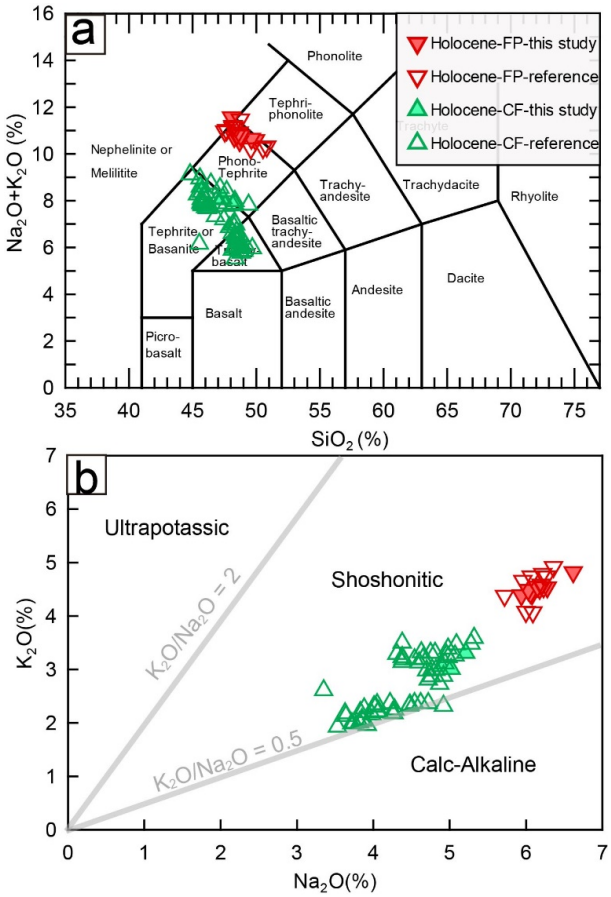

Figure 4. Classification of Holocene lava samples from Jingpohu volcanic field: (**a**) SiO_2 versus $Na_2O + K_2O$, (**b**) Na_2O versus K_2O. Diagrams (**a**,**b**) are modified after [24,25]. For comparison, literature data of Holocene Jingpohu samples [2,26–28] are also plotted.

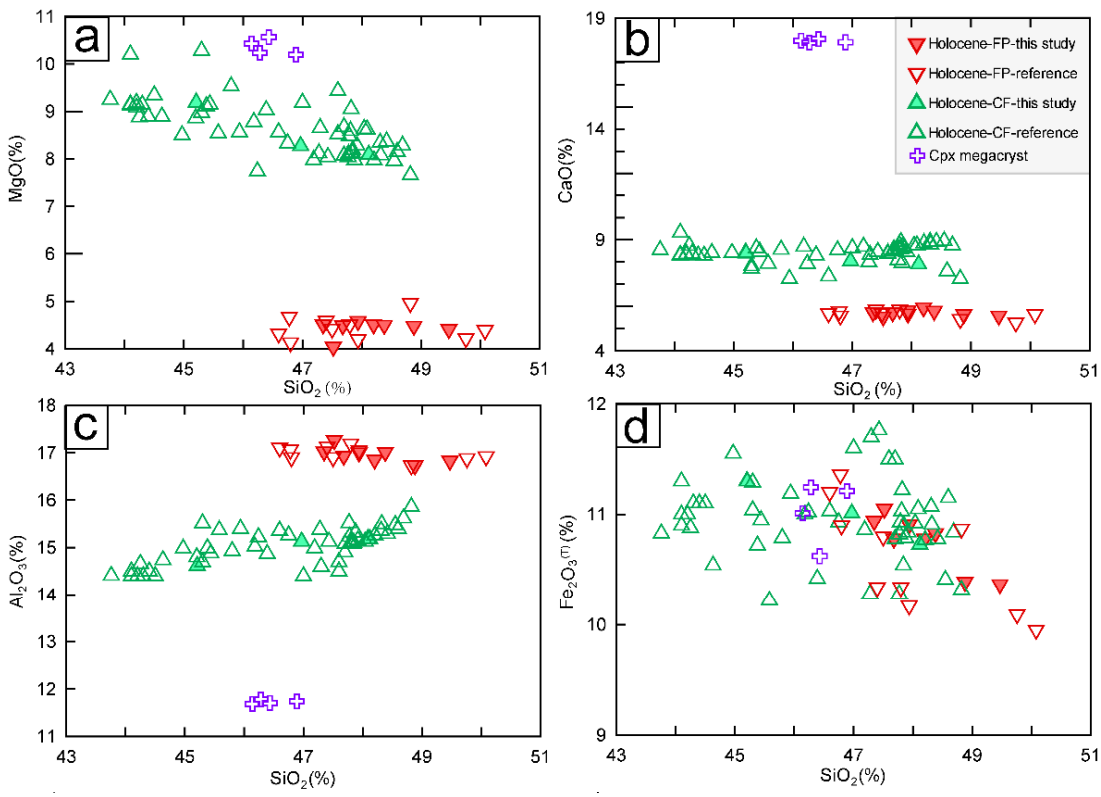

Figure 5. *Conts.*

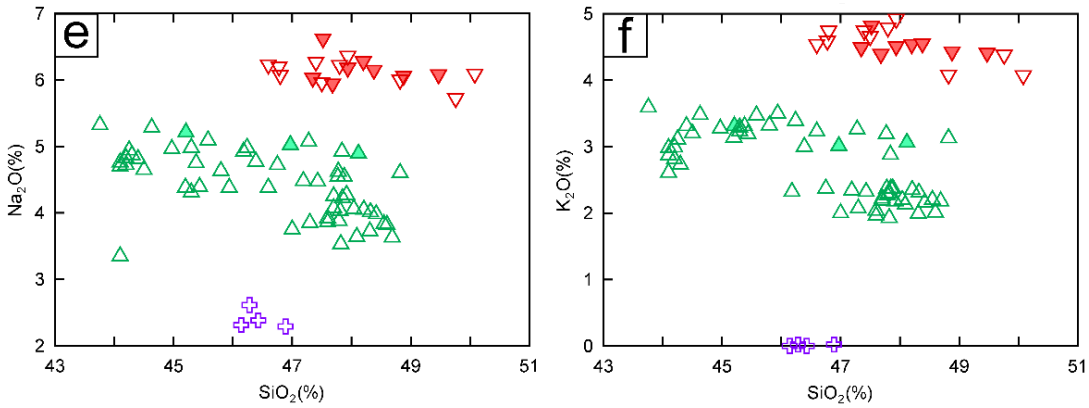

Figure 5. SiO_2 versus MgO (**a**), CaO (**b**), Al_2O_3 (**c**), Fe_2O_3(T) (**d**), Na_2O (**e**), and K_2O (**f**) diagrams for Holocene Jingpohu samples. Compositions of clinopyroxene (Cpx) megacrysts in the FP lavas are from [23].

4.3. Whole-Rock Trace Elements

Whole-rock trace elements of the Holocene Jingpohu samples are presented in Table 1 and in Figure 6. As illustrated by the primitive mantle-normalized spider diagram (Figure 6a), the Jingpohu samples exhibit more enriched patterns than an oceanic island basalt (OIB), but share some of its characteristics, including an absence of negative Nb-Ta anomalies. A chondrite-normalized rare earth element (REE) diagram (Figure 6b) shows that Jingpohu samples are characterized by enriched light rare earth elements (LREE) relative to heavy rare earth elements (HREE). Compared with each other, the FP samples exhibit slightly higher concentrations of large-ion lithophile elements (LILE) and lower HREEs than those of CF samples (Figure 6).

FP samples are also slightly more LREE enriched than CF samples, as shown by somewhat higher La_n and especially by higher $(La/Yb)_n$ ratios (subscript n denotes to their normalization with a primitive mantle), which for both suites, correlate negatively with SiO_2 contents (Figure 7a,b). Samples do not exhibit evident Eu anomalies, with Eu/Eu* = 0.93–1.07 ($Eu/Eu^* = Eu_n \times 2/(Sm_n + Gd_n)$). The Jingpohu samples have Ti/Ti* ratios that range from 0.57 to 0.9 ($Ti/Ti^* = Ti_n \times 2/(Eu_n + Tb_n)$) but without any correlation with SiO_2.

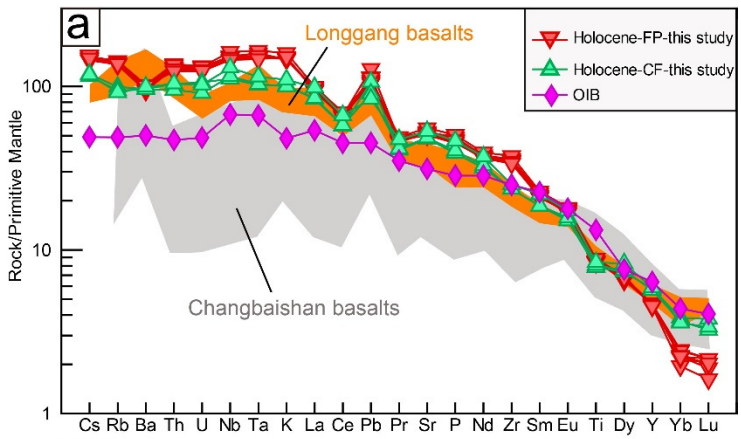

Figure 6. *Conts.*

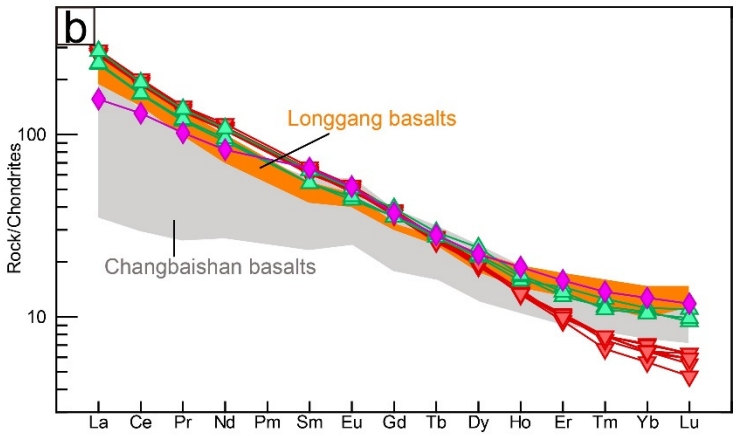

Figure 6. Primitive mantle-normalized incompatible element (**a**) and chondrite-normalized rare earth element diagrams (**b**). Ocean island basalt (OIB) [29] and lavas from Changbaishan [11] and Longgang [2] volcanic fields are presented for comparison. Values of primitive mantle and chondrite are from [29].

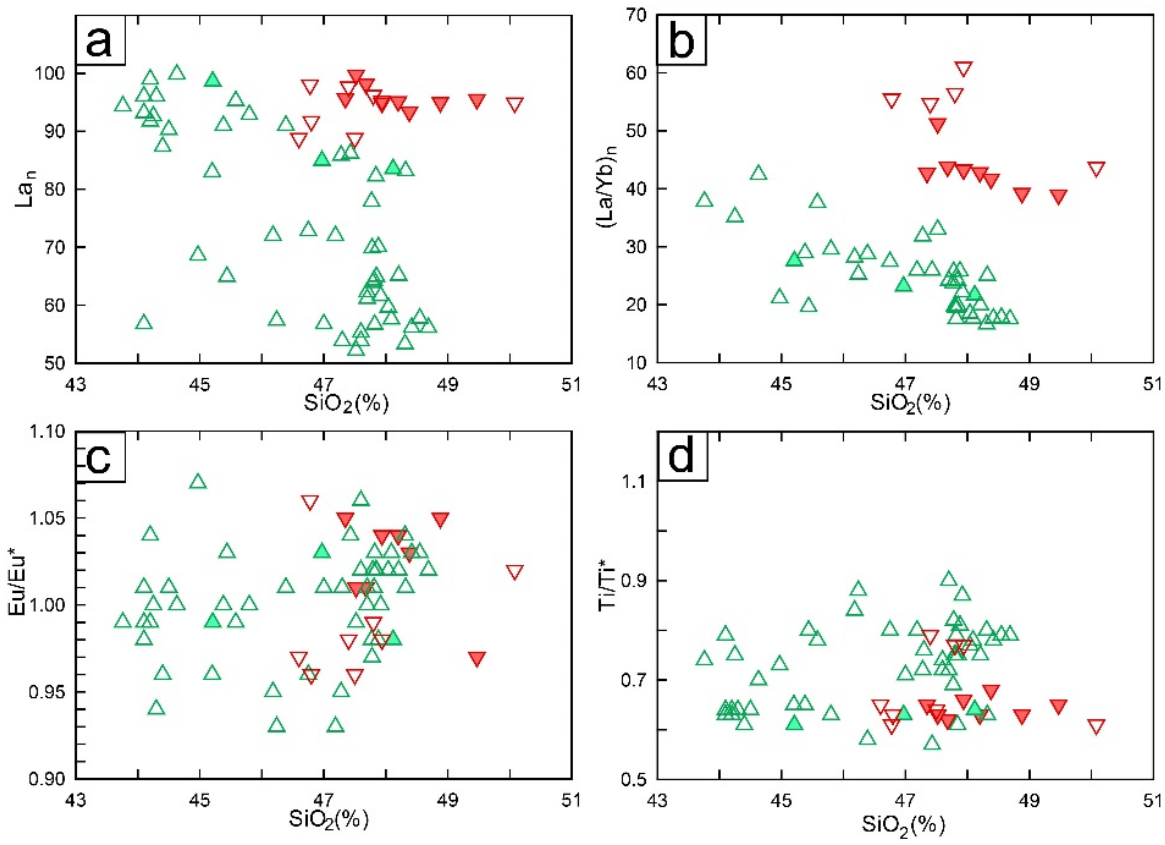

Figure 7. REE characteristics plotted against SiO_2: (**a**) Primitive mantle-normalized La ratios (La_n); (**b**) primitive mantle-normalized La/Yb ratios ($(La/Yb)_n$); (**c**) Eu anomaly (Eu/Eu*). $Eu/Eu^* = Eu_n \times 2/(Sm_n + Gd_n)$. (**d**) Ti anomaly (Ti/Ti*). $Ti/Ti^* = Ti_n \times 2/(Eu_n + Tb_n)$. Literature data and symbols as in Figure 4.

4.4. Whole-Rock Sr-Nd-Pb-Ca Isotopes

Table 2 presents the whole-rock Sr-Nd-Pb-Ca isotopes of the Holocene lavas from Jingpohu volcanic field together with the USGS and other reference materials. For comparison, these are presented together with other published isotopic data on the Jingpohu as well as other sodic and potassic volcanic fields in NE China. As shown in Figure 8a, the Holocene lavas from Jingpohu volcanic area exhibit depleted Sr and Nd isotopes relative to a bulk silicate earth (BSE) [30], with $^{87}Sr/^{86}Sr$ ratios from 0.703915 to 0.704556 and $^{143}Nd/^{144}Nd$ ratios from 0.512656 to 0.512849. The Jingpohu samples are more enriched in Sr-Nd isotopes than the sodic lavas from Changbaishan and Longgang volcanic fields and the potassic lavas. The Jingpohu lavas have $^{208}Pb/^{204}Pb$, $^{207}Pb/^{204}Pb$, and $^{206}Pb/^{204}Pb$ ranges of 37.79–38.06, 15.45–15.54, and 17.49–18.15, respectively (Figure 8b,c). $\delta^{44/40}Ca$ values were calculated by multiplying the $\delta^{44/42}Ca$ values with the slope of an exponential mass-dependent fractionation (2.0483) [30], and result in values that range from 0.63‰ to 0.77‰ and are lower than that of the BSE (0.94 ± 0.05‰; Figure 8d) [31]. Additionally, the CF and FP samples have overlapping Sr-Nd-Pb-Ca isotopic characteristics.

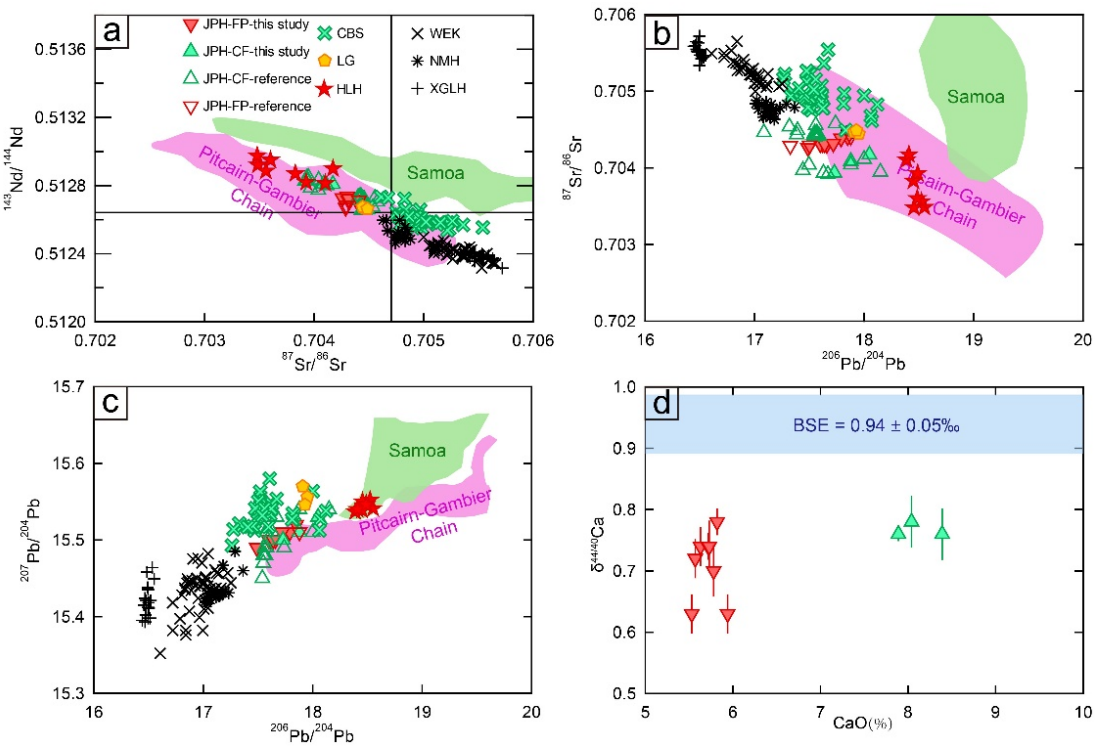

Figure 8. $^{87}Sr/^{86}Sr$ versus $^{143}Nd/^{144}Nd$ (**a**), $^{87}Sr/^{86}Sr$ versus $^{206}Pb/^{204}Pb$ (**b**), $^{207}Pb/^{206}Pb$ versus $^{206}Pb/^{204}Pb$ (**c**), and $\delta^{44/40}Ca$ versus CaO contents (**d**) for Holocene Jingpohu lavas. Literature data of Cenozoic sodic lavas from Jingpohu (JPH), Changbaishan (CBS), Longgang (LG), and Halaha (HLH) volcanic fields and potassic lavas from Wudalianchi–Erkeshan–Keluo (WEK), Nuomihe (NMH), and Xiaogulihe (XGLH) are presented for comparison (detailed references are listed in Supplementary Table S1). The field for EM I-type (magenta; Pitcairn–Gambier Chain) and EM II-type oceanic island basalts (green; Samoa) are from the GEOROC database (http://georoc.mpch-mainz.gwdg.de/georoc/ accessed on 3 March 2021). The $\delta^{44/40}Ca$ value for bulk silicate earth (0.94 ± 0.05‰) is from [31].

Table 2. Whole-rock Sr-Nd-Pb-Ca isotopes of the Holocene lavas from Jingpohu volcanic field.

Sample	Location	$^{87}Sr/^{86}Sr$	2σ	$^{143}Nd/^{144}Nd$	2σ	$^{208}Pb/^{204}Pb$	$^{207}Pb/^{204}Pb$	$^{206}Pb/^{204}Pb$	$\delta^{44/42}Ca$ (‰)	2SD	$\delta^{44/40}Ca$ (‰)	2SD
WJ-1	FP	0.704403	0.000006	0.512720	0.000007	38.051	15.519	17.849	0.35	0.03	0.72	0.07
WJ-2	FP	0.704385	0.000012	0.512715	0.000005	38.011	15.514	17.793	0.36	0.03	0.74	0.06
WJ-3	FP	0.704311	0.000010	0.512730	0.000006	37.921	15.501	17.619	0.36	0.02	0.74	0.04
WJ-4	FP	0.704311	0.000009	0.512726	0.000006	37.907	15.500	17.603	0.36	0.04	0.73	0.09
WJ-5	FP	0.704301	0.000008	0.512737	0.000005	37.941	15.504	17.658	0.31	0.03	0.63	0.06
WJ-6	FP	0.704259	0.000008	0.512727	0.000008	37.849	15.491	17.487	0.31	0.03	0.63	0.05
WJ-7	FP	0.704311	0.000009	0.512715	0.000007	37.929	15.504	17.639	0.38	0.02	0.77	0.05
WJ-8	FP	0.704317	0.000010	0.512723	0.000006	37.976	15.509	17.721	0.34	0.04	0.70	0.08
WJ-9	CF	0.704171	0.000011	0.512808	0.000005	38.057	15.532	18.050	0.37	0.01	0.76	0.01
WJ-10	CF	0.704086	0.000009	0.512809	0.000009	37.962	15.515	17.880	0.38	0.04	0.77	0.09
WJ-11	CF	0.703933	0.000009	0.512831	0.000007	37.888	15.498	17.733	0.37	0.04	0.77	0.08
BCR-2		0.705000	0.000006	0.512644	0.000005	38.744	15.629	18.763	0.40	0.02		
AGV-2		0.703960	0.000006	0.512796	0.000005	38.551	15.621	18.763				
BHVO-2									0.38	0.03		
NIST SRM 915b									0.37	0.03		
Seawater									0.94	0.04		

5. Discussion

5.1. Crustal Assimilation and Fractional Crystallization

During magma ascent, fractional crystallization may modify the chemical compositions of the parental magma and can be evaluated through correlations with a geochemical differentiation index. The presence of anorthoclase, phlogopite, and clinopyroxene megacrysts in the FP lavas suggests that these magmas experienced prolonged durations of medium- to high-pressure crystallization before eruption [23], which would likely also allow for fractionation at depth. Thus, the negative Ba anomalies of FP lavas (Figure 6a) are likely the result of anorthoclase fractionation, while it is otherwise difficult to specify any other fractionating phase in this way. Neither of the two suites exhibit any significant Eu anomaly, negating the fractionation of plagioclase (Figure 7c). Both suites exhibit weak correlations between SiO_2 and other elements, such as MgO, Al_2O_3, Na_2O, K_2O, and La in Figures 5 and 7, indicating some degree of fractional crystallization that could potentially also relate to different proportions of mega/phenocrysts. In contrast, there are no obvious correlations between SiO_2 and $Fe_2O_3^{(T)}$ (Figure 5d) or Ti anomaly (Figure 7d), which preclude any systematic involvement with oxides.

Due to the distinct compositional differences between the crust and mantle-derived magmas, crustal assimilation could also explain some of the chemical and isotopic variations exhibited by Holocene Jingpohu samples. However, their low SiO_2 contents (Figure 5), depleted Sr-Nd isotopes (Figure 8), and lack of any negative Nb-Ta anomalies (Figure 6a) are all inconsistent with any significant contributions of crustal assimilation.

5.2. Differences between the CF and FP Lavas

Carbon-14 dating results showed that the CF and FP lavas in the Jingpohu volcanic field erupted synchronously between 5200 and 5500 years BP [16,17]. However, even though both suites have similar Sr-Nd-Pd-Ca isotope signatures, each has distinctly different geochemical characteristics, including lower MgO and CaO contents and higher Al_2O_3, Na_2O, and K_2O contents of FP lavas compared to those of the CF lavas. Since clinopyroxene megacrysts—only found in FP lavas—also exhibited an opposite higher MgO and CaO contents and lower Al_2O_3, Na_2O, and K_2O contents (Figure 5), yet had comparable SiO_2 contents, we suggest that the geochemical differences between the CF and FP lavas can mainly be attributed to FP lavas having experienced high-pressure clinopyroxene fractionation, while more primitive CF trachybasalts-basanites never crystallized clinopyroxene at depth. Although clinopyroxene is also commonly more HREE-enriched relative to LREEs [32], clinopyroxene fractionation modeling cannot alone lower HREEs as much as observed in the FP lavas. An alternative interpretation for the fractionated HREEs is different partial melting degrees of a garnet-bearing source, which is also consistent with negative correlations between SiO_2 and La_n and $(La/Yb)_n$ (Figure 7a,b). This scenario can also explain the relatively large SiO_2 variation (43.76–50.08%), while most other oxides remain almost constant (Figure 5). Additional fractionation of anorthoclase is needed to also explain the negative Ba anomaly exhibited by FP lavas.

Bai et al.'s review [13] of Jingpohu lavas attributed the lower HREE of FP lavas to an eclogite-bearing peridotite source, while the CF lavas were derived from a garnet peridotite. However, since magmas from different sources are likely to inherit different isotopic characteristics, we prefer to think that the coeval CF and FP suites acquired their geochemical differences after having been derived from a common source assemblage. Therefore, based on geochemical differences, we suggest that the CF and FP lavas originated from a same garnet-bearing source experiencing different melting degrees, while the FP lavas further fractionated clinopyroxene and anorthoclase megacrysts at depth and before eruption.

5.3. Mantle Petrogenesis for the Sodic Lavas

The Holocene Jingpohu lavas exhibit low SiO_2 contents and K_2O/Na_2O ratios that make these sodic as opposed to Nuomihe and Wudalianchi–Erkeshan–Keluo's potassic suites (Figure 4b). While samples exhibit steeper incompatible element patterns than OIBs (Figure 6), with $(La/Yb)_n$ ratios between 16.6 and 61.0 (Figure 7b), they have similar depleted Sr-Nd isotopes (Figure 8a) and overall patterns on the primitive mantle-normalized diagram (Figure 6a). These features not only characterize Jingpohu lavas but are shared by Cenozoic sodic lavas from the nearby Changbaishan and Longgang volcanic fields (Figures 6 and 8), suggesting that these three volcanic fields may have similar petrogeneses and mantle sources.

Figure 8a–c compares the Sr-Nd-Pb isotopes of all late Cenozoic lavas from NE China, including potassic ($K_2O/Na_2O > 1$) and sodic suites ($K_2O/Na_2O < 1$), presented in Figure 8 by black and colored symbols, respectively. Potassic suites are plot within the EM I-type OIB area (Pitcairn–Gambier Chain), suggesting a mixture of DM and EM I sources. As shown in Figure 8a, sodic suites exhibit higher $^{143}Nd/^{144}Nd$ ratios than the potassic lavas and lower $^{143}Nd/^{144}Nd$ ratios than the EM II-type OIB (Samoa) at any given $^{87}Sr/^{86}Sr$ ratio. This can be explained by the addition of a third EM II components to the mixing of DM + EM I. The contribution of an additional EM II component is supported by the $^{87}Sr/^{86}Sr$ and $^{207}Pb/^{206}Pb$ versus $^{206}Pb/^{204}Pb$ diagrams (Figure 8b,c). Additionally, sodic suites are spatially distributed between a DM + EM I domain in the north and a DM + EM II domain in the south, suggesting that the sodic lavas in NE China were derived from up to three different sources: DM, EM I, and EM II.

5.4. Identifying the Origins of the Three Mantle Components

5.4.1. Origin of the DM Source

Both the lithospheric and asthenospheric upper mantle are possible depleted endmember sources beneath NE China. The Cenozoic sodic lavas from Halaha volcanic field (Figure 1), exhibiting the most depleted Sr-Nd isotopes and positive Nb-Ta and negative Pb anomalies, are identified as representing the depleted asthenospheric mantle endmember [4,9]. For Cenozoic potassic lavas, on the other hand, mixing lines between an enriched component (EM I) and the lithosphere on K/U and Hf/*Hf versus $^{87}Sr/^{86}Sr$ and $^{206}Pb/^{204}Pb$ diagrams suggest a depleted lithospheric endmember [4]. However, by adding sodic suites to the plots, stronger mixing lines between the EM I and a depleted asthenosphere (represented by the Halaha lavas) are achieved (Figure 9). This can be explained by the enriched components having significantly higher Sr and Pb concentrations than those of the depleted component and, thereby, allowing relatively small additions of the enriched components to significantly modify Sr and Pb isotopes, while not influencing K/U and Hf/*Hf ratios as much. A depleted asthenospheric source is further supported by tomographic images that reveal an upwelling upper mantle, triggered by a westward subduction and levelling of the Pacific slab on top of the 660 km discontinuity [14,33], which could, thereby, induce decompressional melting. More importantly, xenoliths from the lithospheric mantle beneath the Changbaishan and Longgang volcanic fields exhibit obvious EM II (Figure 10) [34,35], rather than depleted mantle signatures. Notably, sodic suites (colored symbols) exhibit mixing lines that differ from potassic suites (black symbols) and may in fact be the only ones associated with a lithospheric EM II component (Figure 9). Since xenoliths from the lithospheric mantle beneath Changbaishan and Longgang volcanic fields exhibit similar EM II signatures (Figure 10) [34,35], this not only adds a third component to the mix, but also argues for the depleted component to be asthenospheric. Therefore, we propose that the depleted components in all of NE China's Cenozoic volcanoes were sourced from an upwelling asthenospheric, rather than the lithospheric mantle.

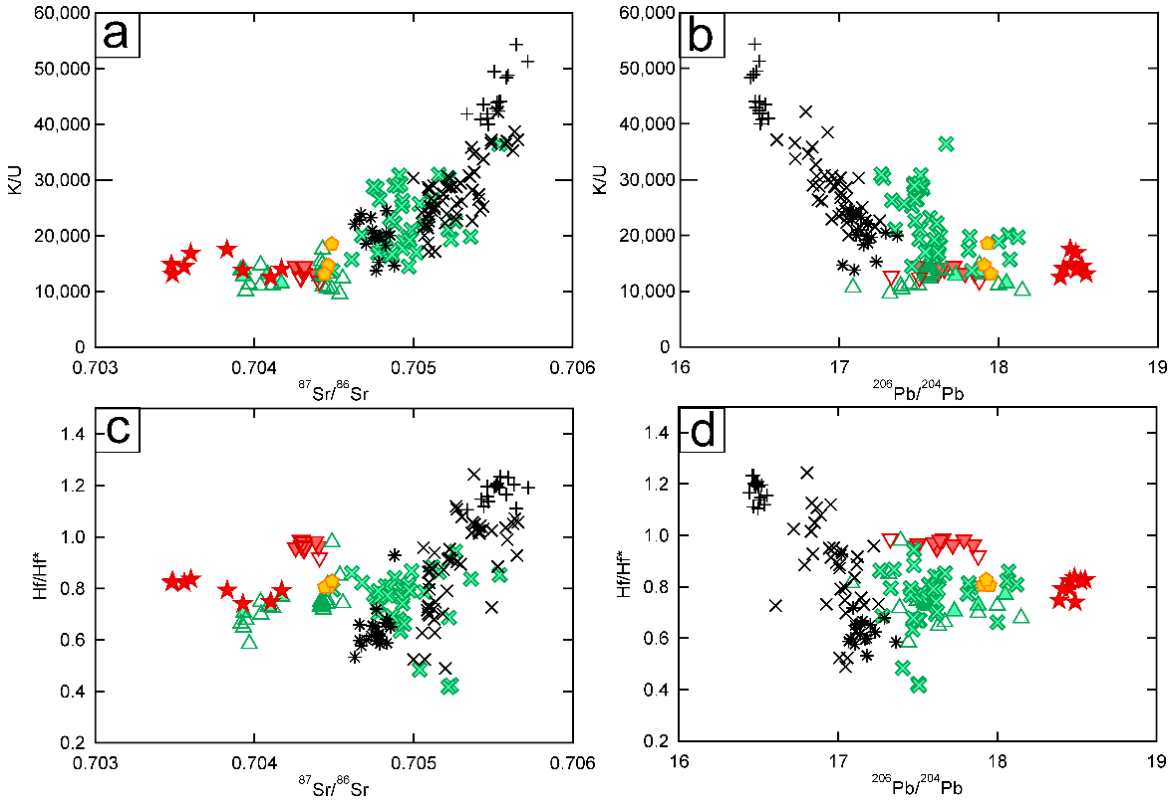

Figure 9. Variations in K/U (**a**,**b**) and Hf/Hf* (**c**,**d**) versus $^{87}Sr/^{86}Sr$ and $^{206}Pb/^{204}Pb$ ratios for Cenozoic sodic and potassic lavas in NE China. Hf/Hf* = $Hf_n/(Sm_n \times Nd_n)^{0.5}$, where subscript donates primitive mantle-normalized value. Literature data and symbols are as in Figure 8.

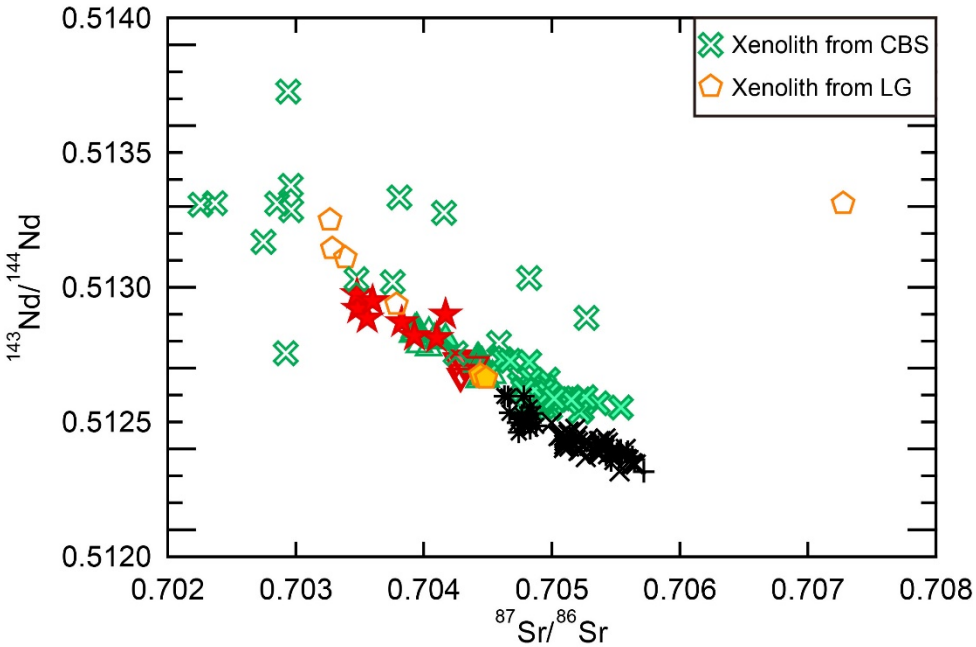

Figure 10. $^{87}Sr/^{86}Sr$ versus $^{143}Nd/^{144}Nd$ ratios of peridotite xenolith entrained in the Cenozoic lavas from Changbaishan and Longgang volcanic fields. Isotopic data of the lavas are also plot for comparison. CBS = Changbaishan, LG = Longgang. Literature data and symbols of the lavas are as in Figure 8.

While the Halaha lavas are thought to most closely represent the depleted asthenosphere [4,8], their overlap with Jingpohu lavas in the Sr-Nd isotopic diagram (Figure 8a) exposes another insight. Thus, since the Jingpohu lavas record a $\delta^{44/40}$Ca range from 0.63‰ to 0.77‰, which is significantly lower than that of a BSE (0.94 ± 0.05‰) [31], this argues for their derivation from a source that was more enriched than a typical depleted asthenospheric upper mantle. Even though the Halaha lavas exhibit negative Pb anomalies, whereas the Jingpohu lavas display positive Pb anomalies, their other geochemical similarities to OIB [4,8] and overlap in the Sr-Nd isotopic diagram (Figure 10) suggest that even the depleted source of the Halaha lavas has been metasomatized by an enriched component. Therefore, we propose the depleted DM asthenosphere must be even more depleted than the Halaha and Jingpohu lavas.

5.4.2. Origin of the EM I Component

Both the potassic and sodic lavas from NE China are plotted within or close to the EM I-type OIB area (represented by Pitcairn–Gambier Chain basalts; Figure 8), implying a larger contribution from this EM I component. Prior to the seismic detection of the Pacific slab beneath NE China [36], studies attributed the EM I components to either the continental lithosphere or recycled sediments in a mantle plume. For example, Zhang et al. [9] suggested that Cenozoic potassic lavas in NE China were produced by partial melting of phlogopite-bearing garnet peridotite in the lithosphere. This inference provided a good explanation for the potassic lavas, which often host phlogopite-bearing peridotite xenoliths, while hydrous phases are absent in mantle xenoliths entrained in the sodic lavas from Changbaishan and Longgang lavas. As mentioned, however, their lithospheric peridotite xenoliths have an EM II Sr-Nd isotope signature (Figure 10) [34,35], rather than EM I, and it is, therefore, unlikely for the EM I component to have originated from the lithospheric mantle.

Based on similar Sr-Nd-Pb isotopic characteristics between the Jingpohu and Hawaii basalts, Zhang et al. [27] proposed a mantle plume source for the Jingpohu lavas. In this scenario, the plume brought up recycled lower crustal materials from the lower mantle, which released enriched fluids that metasomatized the lithospheric mantle. Consequently, they suggested that the metasomatized lithospheric mantle acquired a mixed character between a depleted mantle and EM I. However, seismic tomography shows that the low-velocity anomaly beneath NE China is shallow, ~700 km deep [37], and its underlying subducted Pacific plate blocks the ascent of any deep-seated mantle plume transporting recycled crust. Furthermore, since ^{3}He predominantly originates from the deep earth [38], deep-seated mantle plumes are distinguished from other shallow sources by their extremely high helium isotope ratios (^{3}He/^{4}He), e.g., 13.7–15.9 Ra from Kilauea volcano [39], while volcanic gases from Changbaishan and Wudalianchi retain much lower ^{3}He/^{4}He < 6 Ra [10,40]. In essence, more recent geophysical and geochemical observations do not support a model where recycled crustal sediments are brought up by a deep mantle plume.

After the Pacific plate was detected beneath NE China (e.g., [36]), several studies have suggested that the EM I component of the sodic lavas originate from fluids released by the subducting plate, e.g., [23]. However, ^{230}Th excesses of the youngest eruptions in NE China strongly argue against such fluid contribution from stagnant Pacific plate [2]. In addition, if the west Pacific plate is the main contributor of an EM I source, volcanoes closer to Japan Trench should be more enriched in Sr-Nd isotopes, which is inconsistent with more distal Wudalianchi volcanoes (approximately 2000 km from Japan Trench), exhibiting a great contribution from the EM I component than more proximal Changbaishan and Jingpohu volcanoes (approximately 1200 km from Japan Trench) (Figure 8a). Besides, it is doubtful that the west Pacific plate can still dehydrate after subducting more than 1200 km beneath NE China [2]. Even if the Pacific plate could still be dehydrating, it would not induce such a distinct EM I signature, where Cenozoic lavas exhibit ^{207}Pb/^{206}Pb ratios that are higher than a meteorite isochron, whereas the ^{207}Pb/^{206}Pb ratio of the Pacific slab is lower than that of the meteorite isochron [41]. Furthermore, potassic lavas in oceanic

arcs are characterized by Ce/Pb < 46.5 (Gill et al., 2004), while potassic lavas in NE China have much higher Ce/Pb > 65. In conclusion, although we cannot completely exclude the dehydration of the west Pacific slab, we do not think it was a major contributor towards the EM I source.

Instead, Cenozoic lavas from NE China retain high Ba/Th and $^{207}Pb/^{206}Pb$ ratios, which are more consistent with a record of more ancient dehydration events (>1 Ga) in the mantle transition zone [42]. By modeling the Pb isotope evolution through time, Wang et al. [4] suggest that the extremely unradiogenic Pb isotopes can be attributed to recycled sediments isolated in the mantle transition zone for ~2.2 Ga. This is also consistent with tomographic images, suggesting that the transition zone is extremely hydrous [43,44]. Therefore, after excluding the possibility of an EM I originating from the lithospheric mantle, a mantle plume, or the Pacific slab, we strongly suggest that the EM I components were derived from recycled sediments that have remained isolated within the mantle transition zone for >1 Ga and, therefore, not recycled with the Pacific plate.

5.4.3. Origin of EM II Endmembers

By comparing the isotopic characteristics of Cenozoic potassic and sodic lavas from NE China, we suggested that additional EM II components were involved in the generation of the sodic lavas. The EM II fingerprint in the Jingpohu and Changbaishan lavas was also revealed by [6,13] based on their recognition of a trend towards an EM II endmember in their isotopic plots, and they proposed that it originated from the Pacific slab. However, EM II fingerprints are too sporadically recognized throughout NE Asia. For example, in South Korea, EM II components were detected in the lavas from Jeju Island, but not in nearby volcanic areas such as Jeongok and Baengnyeong [7]. Therefore, the EM II components are more likely formed through localized processes, rather than large-scale processes such as the west Pacific subduction. Localized volcanic structures within the lithosphere beneath Changbaishan volcano have been identified geophysically [45], but more importantly, xenoliths entrained in Changbaishan and Longgang Cenozoic lavas exhibit, as mentioned, isotopic EM II signatures (Figure 10) [34,35], suggesting that it is lithospheric.

Mantle xenoliths from Changbaishan and Longgang volcanic fields primarily comprise spinel lherzolites, with estimated equilibration temperatures ranging from 750 to 1139 °C, supporting a lithospheric mantle origin [34,35]. Lu-Hf and Sm-Nd model ages of residual clinopyroxene within these mantle xenoliths further suggest that the lithospheric mantle was metasomatized between the Early Proterozoic and Phanerozoic ages [34]. Additionally, decoupling of Sr and Nd isotopes within some xenoliths is consistent with diachronous melt extraction [34], which might have introduced the EM II components to the sodic lavas in NE China. Therefore, we propose that the EM II components most likely originated from the lithospheric mantle that was previously metasomatized during ancient subduction events, prior to the subduction of the West Pacific plate.

5.5. Geodynamic Implications by the Sodic Lavas

Since seismic tomography revealed the west Pacific plate beneath NE China, its subduction process and geodynamic impact remain a hot research topic, e.g., [36,46]. Even though geophysical studies suggest that the westward subduction of the Pacific plate played a significant dynamic role in instigating sodic volcanism within a back-arc-like setting, geochemical studies have not found any important material connections between these [2], as also supported by a volcanic gas study in Changbaishan volcanic field [10].

The hydrous upper mantle, imaged as low-velocity anomaly by seismic tomography [46], is attributed to the upwelling of ancient sediments from the mantle transition zone, rather than from a dehydrating west Pacific slab (Figure 11). These ancient sediments in the mantle transition zone is the main EM I reservoir for sodic volcanism in NE China and may exist mainly as a mantle K-hollandite phase [4,47]. K-hollandite is a major repository of LILE (e.g., K, Rb, Ba, Pb, and LREE) and exists as solid phase throughout the transition zone down to the lower mantle [48]. Subduction of the Pacific slab may have trig-

gered a rise in the mantle above the slab [32] and, thereby, brought these ancient sediments to shallower depth. Ascending within an upwelling upper mantle, the decompressional melting of both the ancient sediments and asthenospheric mantle produced a mixed array of EM I and DM components, respectively. When the mixed EM I + DM melts reached the lithosphere, these may locally have interacted with the lithosphere [49] and acquired an additional third EM II contribution from that (Figure 11).

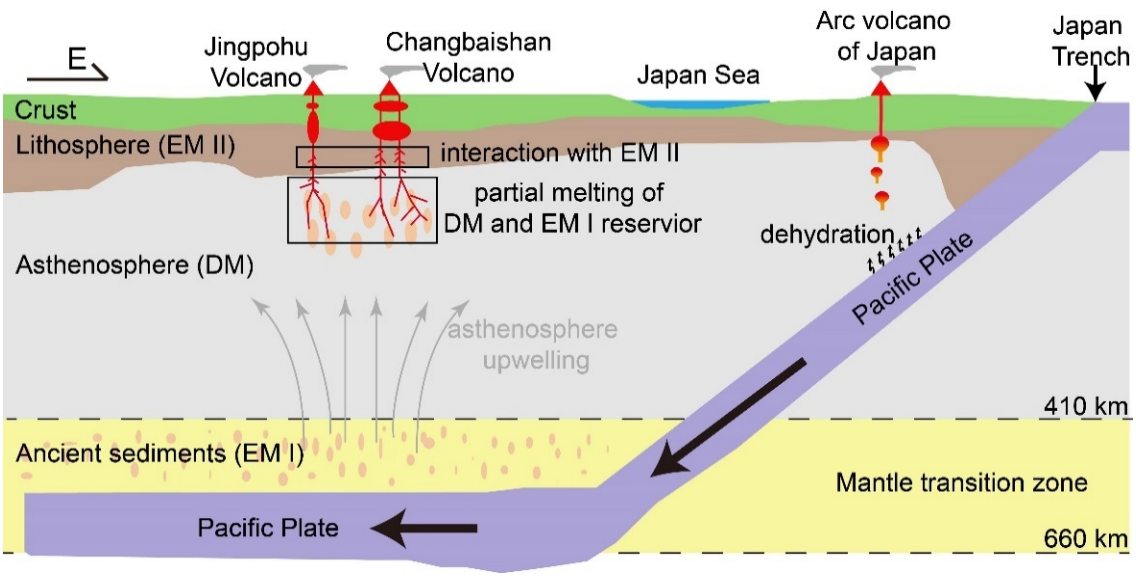

Figure 11. Cartoon showing the three-source model for the Cenozoic sodic lavas in NE China. within the mantle transition zone, ancient sediments (EM I) subducted into the mantle transition zone ~2.2 Ga ago. During Cenozoic, westward subduction of the Paleo-Pacific and Pacific plates caused the upwelling of ancient sediments (EM I). When the ancient sediments (EM I) were brought up to shallower depth, decompression caused partial melting of both ancient sediments (EM I) and their host asthenosphere (DM). Segregated and ascending primary melts interacted with the lithosphere and acquired their EM II signatures from that.

6. Conclusions

New chemical and isotopic data of the Holocene lavas from Jingpohu volcanic field are presented. The main results are summarized as follows.

(1) Jingpohu's Holocene lavas are mainly restricted to the CF and FP volcanic areas. Both FP and CF lavas are otherwise coeval and retain such similar Sr-Nd-Pb-Ca isotopic characteristics, suggesting that they originated from the same sources and experienced similar petrogeneses. The more evolved FP phonotephrites exhibit lower MgO, CaO, and HREEs and higher Al_2O_3, Na_2O, K_2O, and LILEs than those of CF basanites and trachybasalts, which may be attributed to early and high P fractionation of clinopyroxene and anorthoclase, as well as different partial melting degrees of a garnet-bearing source.

(2) By comparing the geochemical characteristics of Jingpohu lavas with other Cenozoic sodic and potassic lavas in NE China, we suggested that sodic lavas originate from three sources, DM, EM I, and EM II, which were derived from the upper asthenosphere, ancient (~2.2 Ga) sediments stored in the mantle transition zone and a locally metasomatized lithospheric mantle, respectively. Isotopic differences between Jingpohu, Changbaishan, and Longgang lavas may be attributed to different proportions of these enriched components during their petrogenesis.

(3) Cenozoic volcanism in NE China was likely triggered by the westward subduction of the Pacific slab, inducing the upwelling and decompressional melting of a transitional mantle with ancient sediments. Even though we cannot completely exclude any

material contributions from the Pacific slab, we do not think it is necessary to explain a varied petrogenesis of Cenozoic magmatism across NE China.

Supplementary Materials: The following are available online at https://www.mdpi.com/article/10.3390/min11080790/s1, Table S1: Chemical and isotopic compositions of the Cenozoic lavas and xenoliths from NE China.

Author Contributions: Conceptualization, F.W. and J.X.; methodology, F.W.; investigation, F.W. and B.P.; writing—original draft preparation, F.W.; writing—review and editing, B.P. and J.X.; project administration, F.W. All authors have read and agreed to the published version of the manuscript.

Funding: This research was funded by the Fundamental Scientific Research Project of Institute of Geology, China Earthquake Administration, grant number IGCEA2013&1820.

Institutional Review Board Statement: Not applicable.

Informed Consent Statement: Not applicable.

Data Availability Statement: Data are available in the Supplementary Table S1.

Acknowledgments: We thank journal editor Aleksandra Milićev and Martin Bromann Klausen and two anonymous reviewers for their constructive comments and suggestions that helped us greatly to improve the manuscript. We are grateful to Li Zhenshan and the staff of Xiaobeihu Forest for their help in the fieldwork.

Conflicts of Interest: The authors declare no conflict of interest.

References

1. Zindler, A.; Hart, S. Chemical geodynamics. *Annu. Rev. Earth Planet. Sci.* **1986**, *14*, 493–571. [CrossRef]
2. Zou, H.; Fan, Q.; Yao, Y. U–Th systematics of dispersed young volcanoes in NE China: Asthenosphere upwelling caused by piling up and upward thickening of stagnant Pacific slab. *Chem. Geol.* **2008**, *255*, 134–142. [CrossRef]
3. Kimura, J.I.; Sakuyama, T.; Miyazaki, T.; Vaglarov, B.S.; Fukao, Y.; Stern, R.J. Plume-stagnant slab-lithosphere interactions: Origin of the late Cenozoic intra-plate basalts on the East Eurasia margin. *Lithos* **2018**, *300–301*, 227–249. [CrossRef]
4. Wang, X.J.; Chen, L.H.; Hofmann, A.W.; Mao, F.G.; Liu, J.Q.; Zhong, Y.; Xie, L.W.; Yang, Y.H. Mantle transition zone-derived EM1 component beneath NE China: Geochemical evidence from Cenozoic potassic basalts. *Earth. Planet. Sci. Lett.* **2017**, *465*, 16–28. [CrossRef]
5. Liu, J.Q.; Chen, L.H.; Zeng, G.; Wang, X.J.; Zhong, Y.; Yu, X. Lithospheric thickness controlled compositional variations in potassic basalts of Northeast China by melt-rock interactions. *Geophys. Res. Lett.* **2016**, *43*, 2582–2589. [CrossRef]
6. Lei, M.; Guo, Z.; Sun, Y.; Zhang, M.; Zhang, L.; Ma, L. Geochemical constraints on the origin of late Cenozoic basalts in the Mt. Changbai volcanic field, NE China: Evidence for crustal recycling. *Int. Geol. Rev.* **2020**, *62*, 2125–2145. [CrossRef]
7. Choi, H.O.; Choi, S.H.; Yu, Y. Isotope geochemistry of Jeongok basalts, northernmost South Korea: Implications for the enriched mantle end-member component. *J. Asian Earth Sci.* **2014**, *91*, 56–68. [CrossRef]
8. Ho, K.S.; Ge, W.C.; Chen, J.C.; You, C.F.; Yang, H.J.; Zhang, Y.L. Late Cenozoic magmatic transitions in the central Great Xing'an Range, Northeast China: Geochemical and isotopic constraints on petrogenesis. *Chem. Geol.* **2013**, *352*, 1–18. [CrossRef]
9. Zhang, M.; Suddaby, P.; Thompson, R.N.; Thirlwall, M.F.; Menzies, M.A. Potassic volcanic rocks in NE China: Geochemical constraints on mantle source and magma genesis. *J. Petrol.* **1995**, *36*, 1275–1303. [CrossRef]
10. Wei, F.; Xu, J.; Shangguan, Z.; Pan, B.; Yu, H.; Wei, W.; Bai, X.; Chen, Z. Helium and carbon isotopes in the hot springs of Changbaishan Volcano, northeastern China: A material connection between Changbaishan Volcano and the west Pacific plate? *J. Volcanol. Geotherm. Res.* **2016**, *327*, 398–406. [CrossRef]
11. Hahm, D.; Hilton, D.; Cho, M.; Wei, H.; Kim, K.R. Geothermal He and CO_2 variations at Changbaishan intra-plate volcano (NE China) and the nature of the sub-continental lithospheric mantle. *Geophys. Res. Lett.* **2008**, *35*. [CrossRef]
12. Choi, H.O.; Choi, S.H.; Lee, Y.S.; Ryu, J.S.; Lee, D.C.; Lee, S.G.; Sohn, Y.K.; Liu, J.Q. Petrogenesis and mantle source characteristics of the late Cenozoic Baekdusan (Changbaishan) basalts, North China Craton. *Gondwana Res.* **2020**, *78*, 156–171. [CrossRef]
13. Bai, X.; Wei, W.; Yu, H.; Chen, Z. Petrogenesis and dynamic implications of the Cenozoic alkali basalts from Jingpohu volcanic field, Northeast China. *Geol. Soc. Lond. Spec. Publ.* **2021**, *510*. [CrossRef]
14. Wei, W.; Zhao, D.; Xu, J.; Wei, F.; Liu, G. P and S wave tomography and anisotropy in Northwest Pacific and East Asia: Constraints on stagnant slab and intraplate volcanism. *J. Geophys. Res. Solid Earth* **2015**, *120*, 1642–1666. [CrossRef]
15. Zhao, D. Tomography and dynamics of Western-Pacific subduction zones. *Monogr. Environ. Earth Planets* **2012**, *1*, 1–70. [CrossRef]
16. Zhang, Z.; Li, Z.; Li, S.; Xin, Y.; Li, Z.; Wang, X.; Yin, J. ^{14}C dating of Holocene volcanic rocks of the Jingpohu Region, Heilongjiang Province, and characteristics of their source regions. *Acta Geol. Sin.* **2000**, *74*, 286. (In Chinese)
17. Fan, Q.; Sun, Q.; Li, N.; Yin, J.; Chen, H.; Gao, F.; Zhang, X. The section of airfall clastic rock of Holocene volcano in Jingpohu region and its eruptive history. *Seismol. Geol.* **2003**, *25*, 3–11. (In Chinese)

18. Zhu, R.; Fu, W.; Meng, L.; Chen, H.; Zhao, Y. Preliminary study on electric structure in the Jingpohu volcano area of the Heilongjiang Province. *Seismol. Geol.* **2001**, *23*, 186–190. (In Chinese)
19. Zou, Z. Electrical Structure Beneath Jingpohu Volcano Area and Its Magmatic Dynamic Significance. Master's Thesis, Jilin University, Changchun, China, 2020.
20. Duan, Y.H.; Zhang, X.K.; Liu, Z.; Yuan, Q.X.; Xu, Z.F.; Wang, F.Y.; Fang, S.M.; Yang, Z.X. Study on crustal structures of Changbaishan-Jingpohu volcanic area using receiver functions. *Chin. J. Geophys.* **2005**, *48*, 389–396. [CrossRef]
21. Fan, X.; Chen, Q.F. Seismic Constraints on the Magmatic System Beneath the Changbaishan Volcano: Insight Into its Origin and Regional Tectonics. *J. Geophys. Res. Solid Earth* **2019**, *124*. [CrossRef]
22. Zhao, J.; Ma, B.; Liang, A.; Li, J.; Gao, S. Analysis on Monitoring capability of volcanic seismic network and the volcanic activity in Jingpohu. *J. Disaster Prev. Reduct.* **2020**, *36*, 57–62. (In Chinese)
23. Fan, Q.; Sun, Q.; Li, N.; Wang, T. Holocene volcanic rock from Jingpohu volcanic field—The diversity of magmas. *Prog. Nat. Sci.* **2005**, *18*, 943–950. (In Chinese)
24. Le Bas, M.J.; Le Maitre, R.W.; Streckeisen, A.; Zanettin, B. A chemical classification of volcanic rocks based on the total alkali-silica diagram. *J. Petrol.* **1986**, *27*, 745–750. [CrossRef]
25. Miller, C.; Schuster, R.; Klötzli, U.; Frank, W.; Purtscheller, F. Post-collisional potassic and ultrapotassic magmatism in SW Tibet: Geochemical and Sr–Nd–Pb–O isotopic constraints for mantle source characteristics and petrogenesis. *J. Petrol.* **1999**, *40*, 1399–1424. [CrossRef]
26. Yan, J.; Zhao, J.X. Cenozoic alkali basalts from Jingpohu, NE China: The role of lithosphere–asthenosphere interaction. *J. Asian Earth Sci.* **2008**, *33*, 106–121. [CrossRef]
27. Zhaochong, Z.; Zong, L.; Zhaonai, L.; Shucai, L.; Zhaomu, L.; Xianzheng, W. Extreme Mantle Heterogeneity beneath the Jingpohu Area, Northeastern China—Geochemical Evidence of Holocene Basaltic Rock. *Acta Geol. Sin. Engl. Ed.* **2000**, *74*, 163–175. [CrossRef]
28. Chen, Y.; Zhang, Y.; Graham, D.; Su, S.; Deng, J. Geochemistry of Cenozoic basalts and mantle xenoliths in Northeast China. *Lithos* **2007**, *96*, 108–126. [CrossRef]
29. Sun, S.S.; McDonough, W.F. Chemical and isotopic systematics of oceanic basalts: Implications for mantle composition and processes. *Geol. Soc. Lond. Spec. Publ.* **1989**, *42*, 313–345. [CrossRef]
30. Farkaš, J.; Déjeant, A.; Novák, M.; Jacobsen, S.B. Calcium isotope constraints on the uptake and sources of Ca2+ in a base-poor forest: A new concept of combining stable (δ44/42Ca) and radiogenic (εCa) signals. *Geochim. Cosmochim. Acta* **2011**, *75*, 7031–7046. [CrossRef]
31. Kang, J.T.; Ionov, D.A.; Liu, F.; Zhang, C.L.; Golovin, A.V.; Qin, L.P.; Zhang, Z.F.; Huang, F. Calcium isotopic fractionation in mantle peridotites by melting and metasomatism and Ca isotope composition of the Bulk Silicate Earth. *Earth. Planet. Sci. Lett.* **2017**, *474*, 128–137. [CrossRef]
32. Bizimis, M.; Salters, V.J.; Bonatti, E. Trace and REE content of clinopyroxenes from supra-subduction zone peridotites. Implications for melting and enrichment processes in island arcs. *Chem. Geol.* **2000**, *165*, 67–85. [CrossRef]
33. Zhao, D.; Tian, Y.; Lei, J.; Liu, L.; Zheng, S. Seismic image and origin of the Changbai intraplate volcano in East Asia: Role of big mantle wedge above the stagnant Pacific slab. *Phys. Earth Planet. Inter.* **2009**, *173*, 197–206. [CrossRef]
34. Park, K.; Choi, S.H.; Cho, M.; Lee, D.C. Evolution of the lithospheric mantle beneath Mt. Baekdu (Changbaishan): Constraints from geochemical and Sr–Nd–Hf isotopic studies on peridotite xenoliths in trachybasalt. *Lithos* **2017**, *286*. [CrossRef]
35. Xu, Q.; Liu, J.; Mo, X.; He, H.; Zhang, Y.; Zhao, W. Characteristics of the lithospheric mantle revealed by peridotite xenoliths from Changbaishan volcanic rocks. *Acta Petrol. Sin.* **2020**, *36*, 2047–2066. (In Chinese)
36. Zhao, D.; Lei, J.; Tang, R. Origin of the Changbai intraplate volcanism in Northeast China: Evidence from seismic tomography. *Chin. Sci. Bull.* **2004**, *49*, 1401–1408. [CrossRef]
37. Tang, Y.; Obayashi, M.; Niu, F.; Grand, S.P.; Chen, Y.J.; Kawakatsu, H.; Tanaka, S.; Ning, J.; Ni, J.F. Changbaishan volcanism in northeast China linked to subduction-induced mantle upwelling. *Nat. Geosci.* **2014**, *7*, 470–475. [CrossRef]
38. Ozima, M.; Podosek, F.A. *Noble Gas Geochemistry*; Cambridge University Press: Cambridge, UK, 2002.
39. Hilton, D.R.; McMurtry, G.M.; Kreulen, R. Evidence for extensive degassing of the Hawaiian mantle plume from helium-carbon relationships at Kilauea volcano. *Geophys. Res. Lett.* **1997**, *24*, 3065–3068. [CrossRef]
40. Xu, S.; Zheng, G.; Nakai, S.I.; Wakita, H.; Wang, X.; Guo, Z. Hydrothermal He and CO_2 at Wudalianchi intra-plate volcano, NE China. *J. Asian Earth Sci.* **2013**, *62*, 526–530. [CrossRef]
41. Hauff, F.; Hoernle, K.; Schmidt, A. Sr-Nd-Pb composition of Mesozoic Pacific oceanic crust (Site 1149 and 801, ODP Leg 185): Implications for alteration of ocean crust and the input into the Izu-Bonin-Mariana subduction system. *Geochem. Geophys. Geosyst.* **2003**, *4*. [CrossRef]
42. Kuritani, T.; Ohtani, E.; Kimura, J.-I. Intensive hydration of the mantle transition zone beneath China caused by ancient slab stagnation. *Nat. Geosci.* **2011**, *4*, 713–716. [CrossRef]
43. Chen, L.; Faccenda, M. Subduction-induced upwelling of a hydrous transition zone: Implications for the Cenozoic magmatism in Northeast China. *J. Geophys. Res. Solid Earth* **2019**, *124*, 11489–11504. [CrossRef]
44. Yang, J.; Faccenda, M. Intraplate volcanism originating from upwelling hydrous mantle transition zone. *Nature* **2020**, *579*, 88–91. [CrossRef] [PubMed]
45. Kim, S.; Tkalčić, H.; Rhie, J. Seismic constraints on magma evolution beneath Mount Baekdu (Changbai) volcano from transdimensional Bayesian inversion of ambient noise data. *J. Geophys. Res. Solid Earth* **2017**, *122*, 5452–5473. [CrossRef]

46. Wei, W.; Xu, J.; Zhao, D.; Shi, Y. East Asia mantle tomography: New insight into plate subduction and intraplate volcanism. *J. Asian Earth Sci.* **2012**, *60*, 88–103. [CrossRef]
47. Choi, H.O.; Choi, S.H.; Schiano, P.; Cho, M.; Cluzel, N.; Devidal, J.L.; Ha, K. Geochemistry of olivine-hosted melt inclusions in the Baekdusan (Changbaishan) basalts: Implications for recycling of oceanic crustal materials into the mantle source. *Lithos* **2017**, *284–285*, 194–206. [CrossRef]
48. Harlow, G.E.; Davies, R. Status report on stability of K-rich phases at mantle conditions. *Lithos* **2004**, *77*, 647–653. [CrossRef]
49. Zhu, H.; Tian, Y.; Zhao, D.; Li, H.; Liu, C. Seismic Structure of the Changbai Intraplate Volcano in NE China from Joint Inversion of Ambient Noise and Receiver Functions. *J. Geophys. Res. Solid Earth* **2019**, *124*, 4984–5002. [CrossRef]